

# Chapter 4

## Luminosity Measurement

### 4.1 Run I Luminosity

The ATLAS Run I data were recorded from 2011 to 2012, with a center-of-mass collision energy of  $\sqrt{s} = 7 \text{ TeV}$  in 2011 and  $\sqrt{s} = 8 \text{ TeV}$  during 2012. Integrated luminosities of  $L = 5.46 \text{ fb}^{-1}$  and  $22.8 \text{ fb}^{-1}$  were delivered by the LHC in the two years, of which  $5.08 \text{ fb}^{-1}$  and  $21.3 \text{ fb}^{-1}$  were recorded by the ATLAS detector. The recorded luminosity accounts for the data acquisition inefficiency, as well as the warm start period, an interval of several minutes after the LHC has declared stable beams during which the tracking detectors are ramped to high voltage and the pixel detector preamplifiers are turned on. After masking data recorded while one or more detector subsystems were not functioning properly,  $4.57 \text{ fb}^{-1}$  and  $20.3 \text{ fb}^{-1}$  of data are considered usable for physics analyses. The volume of delivered, recorded, and physics-ready data are shown as a function of time in figure 4.1a.

The LHC was typically operated with 1042 and 1368 colliding bunches in 2011 and 2012, respectively, with a bunch spacing of 50 ns. The peak instantaneous luminosity reached values as high as  $\mathcal{L} \sim 8 \times 10^{33} \text{ cm}^{-2} \text{ s}^{-1}$ , corresponding to a peak average pileup value of  $\mu \sim 37$ . The distribution of pileup values in 2011 and 2012 data are shown in figure 4.1b.

### 4.2 Measurement Overview

The instantaneous luminosity at a  $pp$  collider is given by [1, 2]:

$$\mathcal{L} = \frac{R_{\text{inel}}}{\sigma_{\text{inel}}}, \quad (4.1)$$

where  $R_{\text{inel}}$  is the rate of inelastic  $pp$  collisions, and  $\sigma_{\text{inel}}$  is the  $pp$  inelastic cross section. For a storage ring with a revolution frequency  $f_r$  and  $n_b$  colliding bunch pairs, the instantaneous luminosity can be written in terms of the average number of inelastic  $pp$  collisions

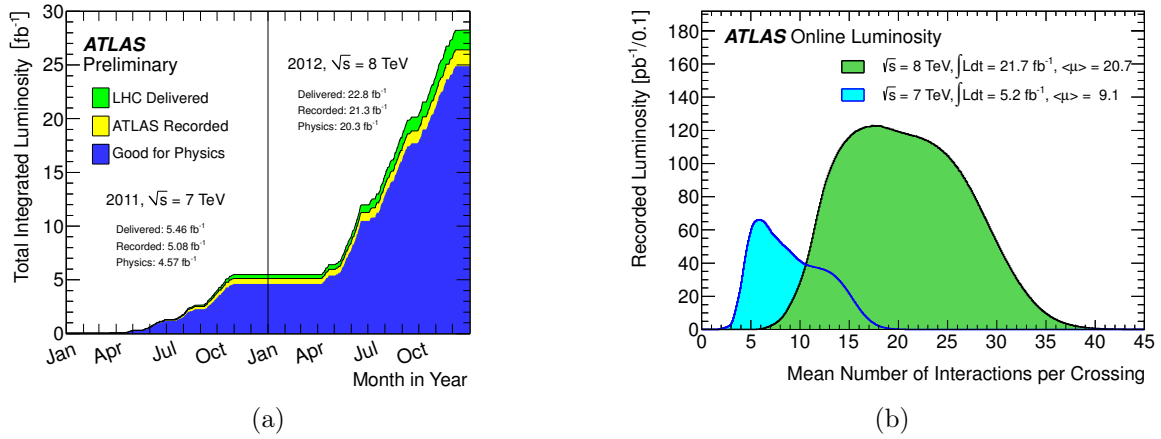


Figure 4.1: Left: The cumulative delivered, recorded, and physics-ready integrated luminosity versus time in 2011-2012. Right: Distribution of the number of interactions per bunch crossing in events recorded in 2011-2012.

per bunch crossing,  $\mu$ , as

$$\mathcal{L} = \frac{\mu f_r n_b}{\sigma_{\text{inel}}}. \quad (4.2)$$

The instantaneous luminosity is measured by ATLAS using several detectors and algorithms, which have some efficiency  $\epsilon$  to detect a  $pp$  interaction and measure the *visible* number of interactions per bunch crossing,  $\mu_{\text{vis}} = \epsilon\mu$ . Defining the visible cross section to be  $\sigma_{\text{vis}} \equiv \epsilon\sigma_{\text{vis}}$ , the instantaneous luminosity as measured by a particular detector is:

$$\mathcal{L} = \frac{\mu_{\text{vis}} f_r n_b}{\sigma_{\text{vis}}}. \quad (4.3)$$

The instantaneous luminosity is measured in intervals of approximately 60 seconds. The visible cross section is a calibration constant for a particular detector, which is determined during dedicated calibration runs in which the luminosity is determined directly from the physical dimensions of the beams. The calibration procedure is described in section 4.4.

### 4.3 Luminosity Detectors

ATLAS performs many redundant luminosity measurements using several detectors. The detectors fall into two categories. *Event counting* detectors have a binary response, returning a 0 or 1 depending on whether a bunch crossing satisfies a set of criteria defined to detect an inelastic  $pp$  collision. Such detectors essentially measure  $p(0; \mu)$ , the probability that an event falls in the zero bin of a Poisson distribution, from which the mean  $\mu$  be calculated. *Hit counting* detectors, on the other hand, count some quantity proportional to the number

of interactions in a given bunch crossing, such as the number of particles identified by a particular detector subsystem. A hit counting measurement typically yields more information about an event at the cost of additional systematic uncertainties.

Ideally, a luminosity detector exhibits the following features:

- The efficiency of the detector should be insensitive to pileup. The visible cross sections are typically measured at  $\mu \approx \mathcal{O}(1)$ , while a typical data-taking run has a peak average pileup of up to  $\mu \sim 40$ ; it is essential that the visible cross section be constant across this range of pileup values.
- The efficiency of the detector should also be constant over long timescales.
- The response of the detector and the readout should fast enough to provide a bunch-by-bunch luminosity measurement. As the LHC bunches are not identical, with different numbers of protons and emittances, it is useful to measure luminosity for each colliding bunch pair, as often as once every 25 ns. The colliding bunch pairs are labeled by the bunch crossing identification number, or BCID, ranging from 1 to 2808; consecutive BCIDs are separated by 25 ns.
- The efficiency should be high enough to yield sufficient statistics. The data are used in increments as short as 20 s, so the statistics collected over this time scale should be high enough that the total uncertainty is dominated by systematic effects. On the other hand, for event counting detectors, the efficiency should not be so high that the detector is saturated; the uncertainty on  $\mu$  is large if  $p(0; \mu)$  is too close to 0 or 1.
- The backgrounds should be low and understandable. Detectors can be sensitive to a wide range of phenomena aside from  $pp$  collisions, which should not be counted as luminosity. For example, some detectors observe a phenomenon called *afterglow*, a small amount of activity in the BCIDs immediately following a collision likely due to photons from nuclear deexcitations in the detector material. The afterglow background is proportional to the luminosity in the colliding BCIDs, and decays away with several time constants. Collisions between a beam and residual gas in the beam pipe, called *beam-gas interactions*, can also contribute a low level of background, and is estimated by observing non-colliding bunches passing through the interaction region.

The central value of the luminosity measurement is determined by the *beam conditions monitor* (BCM) [3], which fulfills most of these desired criteria. The BCM consists of eight diamond-based particle detectors, four on each side of the interaction point at  $|z| = 184$  cm and  $|\eta| = 4.2$ . The detectors have a physical cross section of approximately  $1 \text{ cm}^2$  and are arranged in a cross pattern, with two independent readouts corresponding to the vertical and horizontal pairs. The design purpose of the BCM is to monitor backgrounds and to trigger a beam dump if beam losses towards the inner detector become too high; accordingly, the detector has a very fast readout, and can provide a bunch-by-bunch luminosity measurement

with a time resolution of  $\sim 0.7$  ns. The luminosity is measured using event counting, and can be measured using any combination of the readouts. The configurations used require hits in either the vertical pair (BCM<sub>V</sub>) or the horizontal pair (BCM<sub>H</sub>), and either coincident hits on both sides of the interaction point (AND) or a single hit on either side (OR). The small size of the active sensor leads to an efficiency of approximately 7% in the OR configuration, which allows for sufficient statistics without saturating the detector.

LUCID (LUMinosity measurement using Cherenkov Integrating Detector) [4] provides a supplementary, bunch-by-bunch, event counting-based luminosity measurement. The detector consists of two sets of sixteen Cherenkov detectors surrounding the beampipe at  $z = \pm 17$  m, occupying the pseudorapidity range  $5.6 < |\eta| < 6.0$ . As designed and initially constructed, the Cherenkov detectors are polished aluminum tubes filled with C<sub>4</sub>F<sub>10</sub> gas. The Cherenkov photons induced by charged particles traversing the gas are collected by photomultiplier tubes (PMTs) located at the far end of the tubes. Additional Cherenkov photons are produced in the quartz window separating the tube volume from the PMT. In this configuration, the typical single-particle yield is 60-70 photoelectrons due to photons created in the gas, and about 40 photoelectrons due to the quartz window. A hit is recorded if the PMT signal exceeds a preset threshold, corresponding to about 15 photoelectrons. However, the higher instantaneous luminosities due to the 50 ns bunch spacing led to saturation of the detectors, and hence on 30 July 2011, the gas was removed from the Cherenkov tubes to reduce the efficiency. The removal of the gas also improved the detector's stability and linearity with respect to pileup. Relative comparisons with other detectors were used to reestablish the detector calibration.

Several detector subsystems nominally designed for physics object reconstruction are also used for hit counting-based luminosity measurements. Algorithms using the tile calorimeter and the forward calorimeters (see section 3.2) determine the luminosity from detector currents proportional to the total particle flux in small regions of the calorimeters. The tile calorimeter algorithm monitors the PMT currents corresponding to a few selected cells near  $|\eta| = 1.25$ , where the highest sensitivity to changes in the luminosity is observed. Similarly, the forward calorimeter algorithm monitors the currents in the high voltage lines. In both cases, the detector is unable to provide a bunch-by-bunch measurement, and the current response is not sensitive to the low instantaneous luminosities during the dedicated calibration runs, requiring the calibration to be set using relative comparisons with LUCID or BCM. On the other hand, the detectors exhibit good linearity of response with pileup, and good short-term stability.

Finally, algorithms using the inner detector measure the luminosity by counting reconstructed tracks and vertices<sup>1</sup>. The use of these higher-level objects confers certain benefits, such as low background rates and good long-term stability, at the cost of increased computational requirements, which limit the data rate to  $\mathcal{O}(100 \text{ Hz})$ . Further, pileup effects can be significant; in particular, the efficiency of the vertex counting algorithm varies by as much

---

<sup>1</sup>Pixel cluster counting, used by the CMS experiment, was also considered, but was not commissioned due to the difficulty of the subtraction of the background due to afterglow.

as 30% up to pileup values of  $\mu = 30$ , limiting its utility to data with low pileup.

## 4.4 Luminosity Calibration: van der Meer Scans

The visible cross sections for the detectors and algorithms described in section 4.3 are calibrated during dedicated runs called van der Meer (vdM) scans [5]. The calibration procedure uses the definition of luminosity in terms of the beam parameters, given for a single colliding bunch by:

$$\mathcal{L} = f_r n_1 n_2 K \int \rho_1(x, y, z, t) \rho_2(x, y, z, t) dx dy dz dt, \quad (4.4)$$

where  $f_r$  is the revolution frequency,  $n_{1,2}$  are the number of particles in the colliding bunches, and  $\rho_{1,2}(x, y, z, t)$  are the time- and position-dependent particle density distribution, normalized so that  $\int \rho_{1,2}(x, y, z, t) dx dy dz = 1$ .  $K$  is a kinematic factor,

$$K = \sqrt{(\vec{v}_1 - \vec{v}_2)^2 - \frac{(\vec{v}_1 \times \vec{v}_2)^2}{c^2}}, \quad (4.5)$$

which, in the limit  $|\vec{v}_{1,2}| \rightarrow c$ , reduces to  $2c \cos \alpha$ , where  $\alpha$  is the crossing angle between the beams. To simplify the current discussion, the crossing angle is assumed to be zero, and the bunch densities are assumed to be functions of  $x$ ,  $y$ , and  $z \pm ct$ , i.e. that the transverse bunch profiles are constant over the duration of the collision<sup>2</sup>. The luminosity can then be expressed as:

$$\mathcal{L} = f_r n_1 n_2 \int \hat{\rho}_1(x, y) \hat{\rho}_2(x, y) dx dy, \quad (4.6)$$

where  $\hat{\rho}_{1,2}(x, y)$  are the transverse particle densities, normalized to unity. Under the further assumption that the transverse particle densities factorize in the horizontal and vertical directions,  $\hat{\rho}(x, y) = \hat{\rho}_x(x) \hat{\rho}_y(y)$ , where  $\hat{\rho}_x(x)$  and  $\hat{\rho}_y(y)$  are also normalized to unity, the luminosity can be written as:

$$\mathcal{L} = f_r n_1 n_2 \Omega_x(\hat{\rho}_{x1}, \hat{\rho}_{x2}) \Omega_y(\hat{\rho}_{y1}, \hat{\rho}_{y2}), \quad (4.7)$$

where  $\Omega_x(\hat{\rho}_{x1}, \hat{\rho}_{x2}) = \int \hat{\rho}_{x1}(x) \hat{\rho}_{x2}(x) dx$ , and similarly for the  $y$  direction<sup>3</sup>. As first proposed by van der Meer, the  $\Omega_{x,y}$  parameters can be determined by measuring the interaction

---

<sup>2</sup>In particular, the *hourglass effect* is neglected. The collisions occur in a drift space, where the beams are focused, or squeezed, onto the interaction point. The transverse size of the beam in direction  $i$  as a function of  $z$  is given by  $\sigma_i^2(z) = \epsilon_i \beta_i^* \left(1 + \frac{(z - z_i^w)^2}{\beta_i^{*2}}\right)$ , where  $\epsilon_i$  is the transverse emittance,  $z_i^w$  is location of the optical waist, and  $\beta_i^*$  is the betatron function at  $z = z_i^w$ . The effect is significant when  $\beta_i^* \lesssim \sigma_z$ ; during the vdM scans,  $\sigma_z \approx 50$  mm, while  $\beta^* = 1.5$  m-11 m, and hence the hourglass effect is neglected.

<sup>3</sup>The formalism can be generalized to the case where the beam profiles do not factorize in  $x$  and  $y$ ; see [Balagura:2011er].

rate as a function of transverse beam displacement,  $R_{x,y}(\delta)$ . Without loss of generality, assume that beam 2 is displaced by  $\delta$  in the  $x$  direction, while beam 1 is held fixed. Then,  $R_x(\delta) = k \int \rho_{x1}(x) \rho_{x2}(x - \delta) dx$  for some constant  $k$ , and

$$\frac{R_x(0)}{\int R_x(\delta) d\delta} = \frac{k \int \rho_{x1}(x) \rho_{x2}(x) dx}{k \int \int \rho_{x1}(x) \rho_{x2}(x - \delta) dx d\delta} \quad (4.8)$$

$$= \int \rho_{x1}(x) \rho_{x2}(x) dx \quad (4.9)$$

$$= \Omega_x(\hat{\rho}_{x1}, \hat{\rho}_{x2}) \quad (4.10)$$

For convenience, define  $\Sigma_{x,y}$  to be the characteristic widths of  $R_{x,y}(\delta)$ , given by:

$$\Sigma_{x,y} = \frac{1}{\sqrt{2\pi}} \frac{\int R_{x,y}(\delta) d\delta}{R_{x,y}(0)}. \quad (4.11)$$

For Gaussian beams,  $\Sigma_{x,y}$  correspond to the Gaussian width of  $R_{x,y}(\delta)$ . Finally, the luminosity is given by

$$\mathcal{L} = \frac{f_r n_1 n_2}{2\pi \Sigma_x \Sigma_y}. \quad (4.12)$$

Equating this with the luminosity defined in equation 4.3, the visible cross section for a given detector and algorithm is given by

$$\sigma_{\text{vis}} = \mu_{\text{vis}}^{\text{MAX}} \frac{2\pi \Sigma_x \Sigma_y}{n_1 n_2}, \quad (4.13)$$

where  $\mu_{\text{vis}}^{\text{MAX}}$  is the visible interaction rate per bunch crossing at the maximum of the scan curve,  $R(\delta)$ . The numbers of particles per bunch,  $n_{1,2}$ , are measured by the LHC Bunch Current Normalization Working Group using bunch current transformers (BCTs) [6–8].

## 2011 Luminosity Calibration

As an example, the 2011  $pp$  calibration is derived from two pairs of scans in the  $x$ - and  $y$ -directions, performed during the same LHC fill on 15 May 2011 [2]. The beams had 14 colliding bunch pairs,  $\sim 0.8 \times 10^{11}$  protons per bunch,  $\beta^* = 1.5$  m, and a crossing angle of  $\alpha = 240 \mu\text{rad}$ . The resulting transverse beam size was approximately  $\sigma_x \approx \sigma_y \approx 40 \mu\text{m}$ , and the peak average number of interactions per crossing with head-on collisions was  $\mu \approx 2.3$ . The scan was performed in 25 equal steps over a displacement range of  $\delta = \pm 233 \mu\text{m}$ .

Figure 4.2 shows an example scan curve, with the specific visible interaction rate,  $\mu_{\text{vis}}^{\text{sp}} \equiv \mu_{\text{vis}} / (n_1 n_2)$ , plotted as a function of transverse beam separation for the BCMV\_OR algorithm. Normalizing by the bunch current product,  $n_1 n_2$ , eliminates the dependence of the curve on the decreasing beam currents over the course of the scan. The vdM scan curve is fitted with

a Gaussian plus a constant, which is used as  $R_{x,y}(\delta)$  to calculate  $\Sigma_{x,y}$  in equation 4.11.  $\mu_{\text{vis}}^{\text{MAX}}$  is determined from the peak of the fitted function. The measured  $\sigma_{\text{vis}}$  values for both scans and all 14 colliding bunch pairs are shown in figure 4.3. The luminosity-weighted mean  $\sigma_{\text{vis}}$  is taken as the central value, while the scatter of the 28 measurements, which is not consistent with statistical variation, is taken as a systematic uncertainty on the reproducibility of the measurement.

The visible cross sections for several algorithms using during 2011 are shown in table 4.1, along with the efficiency assuming a total inelastic cross section of  $\sigma_{\text{inel}} = (71.34 \pm 0.90)$  mb [9].

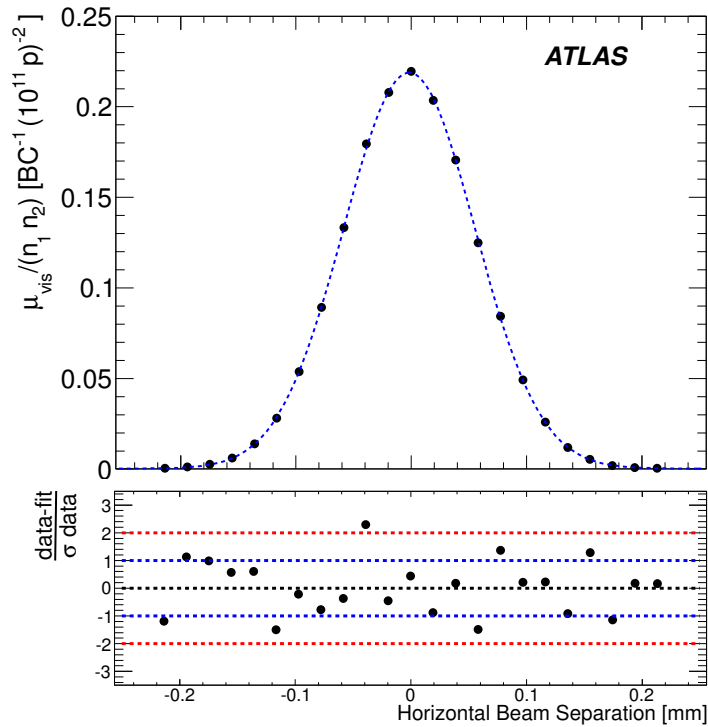


Figure 4.2: An example of a scan curve measured by BCMV\_OR from the van der Meer scans on 15 May 2011. The specific visible interaction rate  $\mu_{\text{vis}}^{\text{sp}} \equiv \mu_{\text{vis}}/(n_1 n_2)$  is shown as a function of transverse beam separation in the  $x$  direction for a single scan and BCID. The data are fitted with Gaussian plus constant. The bottom plot shows the residual deviation of the data from the fit, divided by the uncertainty on the data.

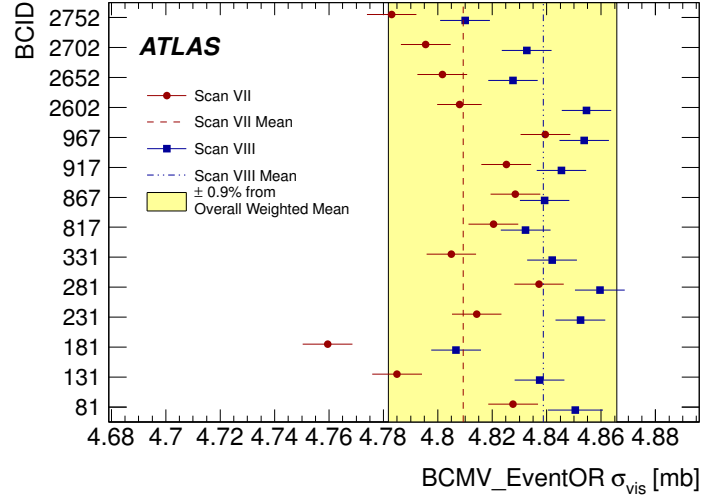


Figure 4.3: Measured  $\sigma_{\text{vis}}$  values from the vdM scans performed in May 2011. The error bars represent statistical uncertainties only. The vertical dashed lines indicate the weighted average over BCIDs from the two sets of scans. The yellow band shows a variation of  $\pm 0.9\%$  from the total weighted average, equal to the systematic uncertainty due to the observed BCID-to-BCID and scan-to-scan variations.

Algorithm	$\sigma_{\text{vis}}$ (2011)	$\frac{\sigma_{\text{vis}}}{\sigma_{\text{inel}}}$
BCM_VOR	$4.82 \pm 0.07$	0.068
BCM_HOR	$4.78 \pm 0.07$	0.067
BCM_VAND	$0.142 \pm 0.002$	0.002
BCM_HAND	$0.140 \pm 0.002$	0.002
LUCID_OR	$43.3 \pm 0.7$	0.607
LUCID_AND	$13.7 \pm 0.2$	0.192

Table 4.1: Visible cross sections for  $pp$  luminosity measurement algorithms used in 2011. The corresponding efficiency of detecting an inelastic  $pp$  collision is also shown for  $\sigma_{\text{inel}} = 71.34 \text{ mb}$ .



## 4.5 Systematic Uncertainties

The systematic uncertainty on the 2011 and 2012 luminosity measurements are 1.8% and 2.8%<sup>4</sup>, respectively. No single source of uncertainty dominates the total; rather, the uncertainty is due to many sources, each contributing less than 1%. The sources of uncertainty on the 2011 luminosity measurement are shown in table 4.2, divided into uncertainties on the visible cross section measurement during vdM scans and uncertainties on the measurement performed over the course of data taking.

The combined uncertainty on the visible cross sections due to the vdM calibration procedure is 1.5%. The largest source of uncertainty is due to emittance growth and non-reproducibility, reflected in the scatter between BCIDs and between scans in figure 4.3. Other significant sources, each roughly 0.5%, include beam-beam effects, where the two colliding beams deflect each other away from the nominal transverse separation; transverse correlations which violate the assumption that the transverse particle densities factorize as  $\rho(x, y) = \rho_x(x)\rho_y(y)$ ; pileup dependence; and the measurement of the number of protons per bunch,  $n_{1,2}$ .

Uncertainties on the luminosity measurement over the 2011 data-taking period total 0.9%. These uncertainties are dominated by variations in the detector efficiencies during 2011, quantified using relative comparisons between algorithms across the entire year, and pileup dependence, quantified using relative comparisons between algorithms at different pileup values. The relative comparisons are shown in figure 4.4.

The sources contributing to the 2.8% systematic uncertainty in 2012 are similar. The 1% increase from 2011 is largely due to long-term consistency: comparisons with tile and forward calorimeter measurements indicate that the BCMV\_OR efficiency drifted with respect to the calorimeters by as much as 2% over the year. The full 2% is taken as a conservative systematic uncertainty.

## 4.6 Vertex-Based Luminosity Measurement

Primary vertices are points consistent with being the origin of a set of tracks reconstructed by the inner detector, nominally due to inelastic  $pp$  interactions. The reconstruction of tracks and vertices is described in section 5.1. Vertex counting [10] is an appealing luminosity measurement technique for a number of reasons. The backgrounds are very low, and can be controlled by requiring a minimum number of tracks per vertex, chosen here to be five tracks with  $p_T > 400$  MeV. Further, the vertex reconstruction efficiency is expected to be stable throughout the data taking period. However, the technique has two significant drawbacks. First, the data is collected through the standard ATLAS data acquisition system, limiting the event rate during normal physics runs to  $\mathcal{O}(100 \text{ Hz})$ . Depending on the trigger used, a correction for the trigger deadtime may also be necessary. Second, the efficiency of the vertex

---

<sup>4</sup>Preliminary uncertainty. The final uncertainty is expected to be around 2%.

Source	Uncertainty	
Bunch population product ( $n_1 n_2$ )	0.5%	} vdM calibration subtotal=1.5% Uncertainties from a single measurement of $\sigma_{\text{vis}}$
Beam centering	0.10%	
Beam position jitter	0.30%	
Emittance growth/non-reproducibility	0.67%	
Bunch-to-bunch $\sigma_{\text{vis}}$ consistency	$\oplus$ 0.55%	
Fit model	0.28%	
Background subtraction	0.31%	
Specific luminosity	0.29%	
Length scale calibration	0.30%	
Absolute ID length scale	0.30%	
Beam-beam effects	0.50%	} $\mathcal{L}$ measurement subtotal=0.9% Uncertainties evaluated from all 2011 physics runs
Transverse correlations	0.50%	
Pileup dependence	0.50%	
Afterglow correction	0.2%	
BCM Stability	0.2%	
Long-term consistency	0.7%	
Pileup dependence	0.5%	
Total	1.8%	

Table 4.2: Systematic uncertainties on the integrated luminosity measured in 2011 using the BCM\_VOR algorithm. The uncertainties are separated into uncertainties on the visible cross section (1.5%) and measurement uncertainties over the year (0.9%).

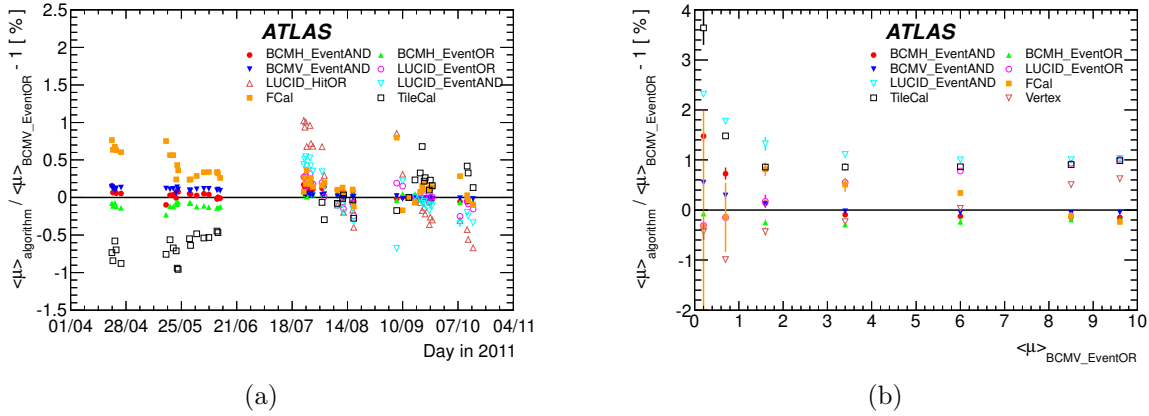


Figure 4.4: Left: Comparison of luminosities measured by different algorithms as a function of time in 2011. Right: Comparison of luminosities measured by different algorithms as a function of the average number of interactions per bunch cross,  $\mu$ , as measured by BCM\_VOR. The data were taken during a single run by separating the beams in the transverse direction, similar to a van der Meer scan.

reconstruction algorithm is significantly nonlinear with pileup, with the efficiency decreasing by  $\sim 30\%$  between pileup values of  $\mu = 1$  and  $\mu = 30$ .

## Vertex Counting Method

The data for the inner detector-based luminosity measurements are collected through the standard ATLAS data acquisition system. Events are collected with either a random trigger or a trigger requiring hits in the minimum bias trigger scintillators (MBTS), two discs of scintillators mounted on the inner surfaces of the LAr end-cap cryostats ( $2.12 < |\eta| < 3.85$ ). Both triggers can select a specific set of BCIDs, which is essential for special runs where a bunch-by-bunch measurement is necessary, e.g. the vdM scans. The random trigger records a fraction of all bunch crossings in a specific set of colliding BCIDs, enabling an unbiased measurement of  $\mu_{\text{vis}}$  at the cost of lower statistics. The statistics collected worsen at low pileup values, where a large fraction of the triggered events do not contain a collision; hence, the random trigger is used mostly at high pileup. At lower pileup, the statistics can be recovered by using the MBTS trigger, which requires a small number of hits in the MBTS, usually at least two. Care must be taken to avoid bias due to the nontrivial trigger requirements: the trigger inefficiency, prescale, and deadtime must be taken into account. For vertices with at least five tracks, the inefficiency is negligible.

Vertices are reconstructed with two settings: the default reconstruction settings based on tracks with  $p_T > 400$  MeV, and tighter settings (“VtxLumi”) based on tracks with  $p_T > 900$  MeV with stricter requirements on the track quality. The tighter settings were introduced in 2012 to reduce the computational requirements associated with collecting  $\mathcal{O}(100 \text{ Hz})$  of inner detector data over the entire year. The studies described below are based on the 2011 data, where the vertex-based luminosity measurement is only performed on special runs, and use the default reconstruction settings.

The single-bunch instantaneous luminosity is calculated as follows. For the random trigger, the visible interaction rate is  $\mu_{\text{vis}} = \frac{N_{\text{vtx}}}{N_{\text{evt}}}$ , where  $N_{\text{vtx}}$  is the number of vertices recorded in  $N_{\text{evt}}$  triggered events. For the MBTS trigger,  $\mu_{\text{vis}} = \frac{N_{\text{vtx}}}{f_r \Delta t}$ , where  $N_{\text{vtx}}$  is the number of vertices recorded after correcting for the prescale and deadtime,  $f_r = 11\,245.5 \text{ Hz}$  is the LHC revolution frequency, and  $\Delta t$  is the duration of the measurement.  $\mu_{\text{vis}}$  is then corrected for pileup effects, described below in section 4.6, and finally the luminosity is given by equation 4.3.

## Pileup Effects

The vertex reconstruction efficiency is strongly affected by three pileup-related phenomena:

- Vertex masking: a  $pp$  interaction fails to be reconstructed as a vertex because some or all of its tracks are used by an earlier vertex in the iterative reconstruction algorithm. This is the dominant pileup effect, which causes a large drop in the reconstruction efficiency at high pileup.

- Fake vertices: a vertex passes the cut on the minimum number of tracks due to acquiring tracks from another nearby  $pp$  interaction. This is a subdominant but significant effect, which causes a small increase in the reconstruction efficiency at high pileup.
- Split vertices: a single interaction is reconstructed as two separate vertices. This is a significant effect when considering vertices with two or more tracks, but is negligible for vertices with at least five tracks.

Corrections are derived for vertex masking and fake vertices. The fake vertex correction is derived using truth matching in minimum bias Monte Carlo simulation. The simulation sample was generated using PYTHIA 8, with tune A2M [11, 12]. For a given cut on the minimum number of tracks per vertex,  $n_{\text{trk,min}}$ , a reconstructed vertex is labelled as fake if less than  $n_{\text{trk,min}}$  of its tracks are matched to charged particles originating from the same generated  $pp$  interaction. The average number of reconstructed vertices labelled as fake by Monte Carlo truth matching is shown as a function of pileup in figure 4.6. The fake fractions show a significant dependence on  $\mu$  and on the  $n_{\text{trk,min}}$ .

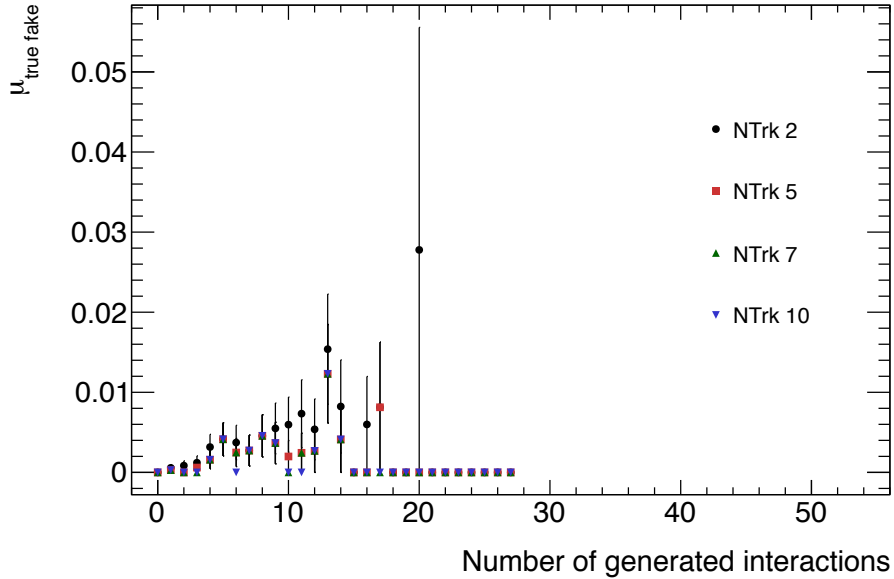


Figure 4.5: Average number of reconstructed vertices without a matched truth interaction, as a function of number of generated interactions per event. The contribution is below 0.1%.

A correction is derived for vertex masking using the distribution of longitudinal distances,  $\Delta z$ , between pairs of vertices in the same event. In the absence of masking, if the interaction region has a Gaussian longitudinal profile with width  $\sigma_z$ , then the  $\Delta z$  distribution would be a Gaussian with width  $\sigma_z \times \sqrt{2}$ . Masking manifests as an absence of reconstructed pairs near  $\Delta z = 0$ , as shown in figure 4.7.

The correction is derived in a data-driven way as follows.

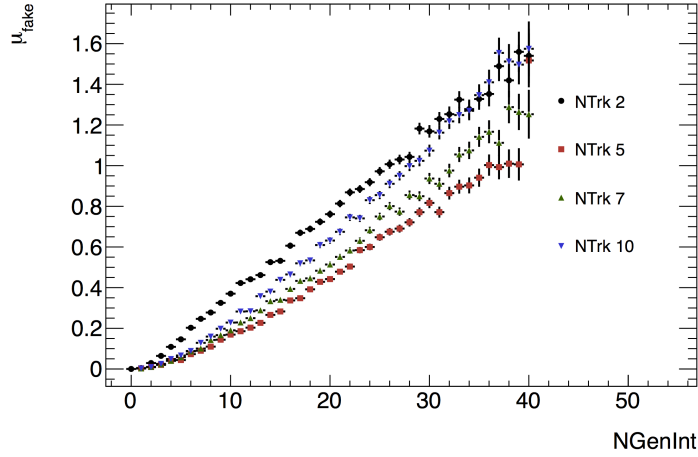


Figure 4.6: Average number of fake vertices per event as a function of the number of generated  $pp$  interactions.

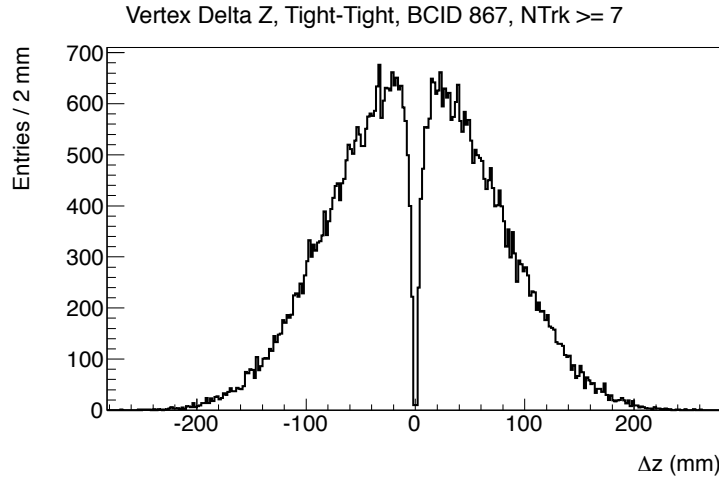


Figure 4.7:  $\Delta z$  distribution between pairs of vertices in the same event, with data from the May Van der Meer scan (ATLAS run 182013).

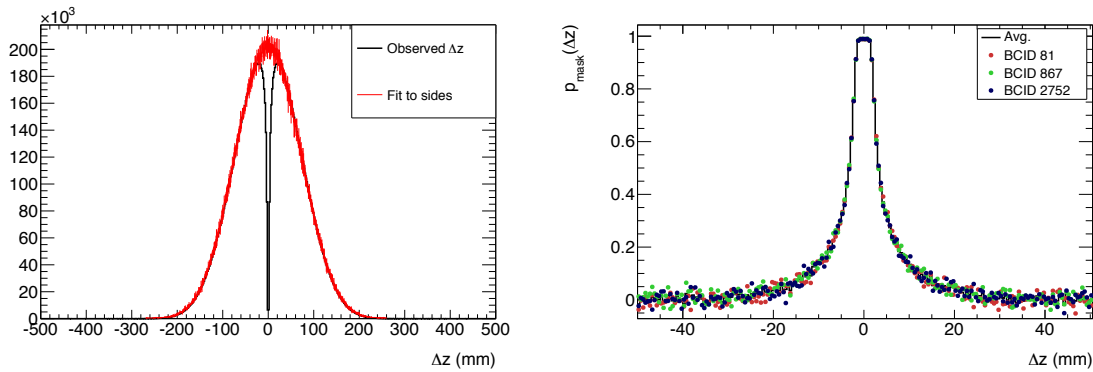
1. In a data sample with exactly two interactions per event, the number of masked pairs is equal to the number of masked vertices. Using data taken at low pileup values and selecting events with exactly two reconstructed vertices, we calculate the 2-vertex masking probability  $p_{\text{mask}}(\Delta z)$ , i.e. the probability that only one of two vertices separated by  $\Delta z$  is reconstructed. This function is assumed to be a universal property of the vertexing algorithm, independent of  $\mu$ .

Specifically, the expected  $\Delta z$  distribution in the absence of masking,  $f_{\text{exp}}(\Delta z)$ , is derived by randomly sampling pairs of points from the observed  $z$ -distribution of reconstructed vertices. Using  $f_{\text{exp}}(\Delta z)$  as a template, the *observed*  $\Delta z$  distribution,

$f_{\text{obs}}(\Delta z)$ , is fitted in the range  $30 \text{ mm} \leq |\Delta z| \leq 300 \text{ mm}$ , where vertex masking is negligible. Finally, the masking probability is defined as:

$$p_{\text{mask}}(\Delta z) = \frac{f_{\text{exp}}(\Delta z) - f_{\text{obs}}(\Delta z)}{f_{\text{exp}}(\Delta z)} \quad (4.14)$$

The masking probability functions derived from minimum bias Monte Carlo and for low- $\mu$  data are shown in figures 4.8 and 4.9.



(a)  $\Delta z$  distribution and template fit, NTrk5, BCID  
81

(b)  $p_{\text{mask}}(\Delta z)$ , NTrk5

Figure 4.8: Calibration of the masking correction method on data, using run 182013. Left:  $\Delta z$  distributions and template fits using expected  $\Delta z$  distributions in the range  $30 \text{ mm} \leq \Delta z \leq 300 \text{ mm}$ . Right: pairwise vertex masking probability as a function of the longitudinal distance  $\Delta z$  between the vertices.

2. To derive a correction for a particular data sample at arbitrary  $\mu$ , an *expected*  $\Delta z$  distribution,  $f_{\text{exp}}(\Delta z)$ , is again derived by randomly sample pairs of vertices from the observed primary vertex  $z$ -distribution. Then, the total probability  $p_{\text{mask}}$  that given any two tight vertices, only one is reconstructed can be computed:

$$p_{\text{mask}} = \int_{-\infty}^{\infty} p_{\text{mask}}(\Delta z) f_{\text{exp}}(\Delta z) d(\Delta z). \quad (4.15)$$

3. The total masking probability  $p_{\text{mask}}$  is used to generate a map between the number of reconstructible vertices per event,  $N_{\text{vis}}$ , and the average number of reconstructed vertices per event,  $\mu_{\text{rec}}$ , as follows. Label the generated vertices  $v_i$ ,  $1 \leq i \leq N_{\text{gen}}$ , in the order in which the iterative vertexing algorithm reconstructs the vertices; similarly, let  $p_i$ ,  $1 \leq i \leq N_{\text{vis}}$ , be the probability that vertex  $v_i$  is reconstructed. Proceeding vertex-by-vertex, the  $p_i$  follow a recursion relation:

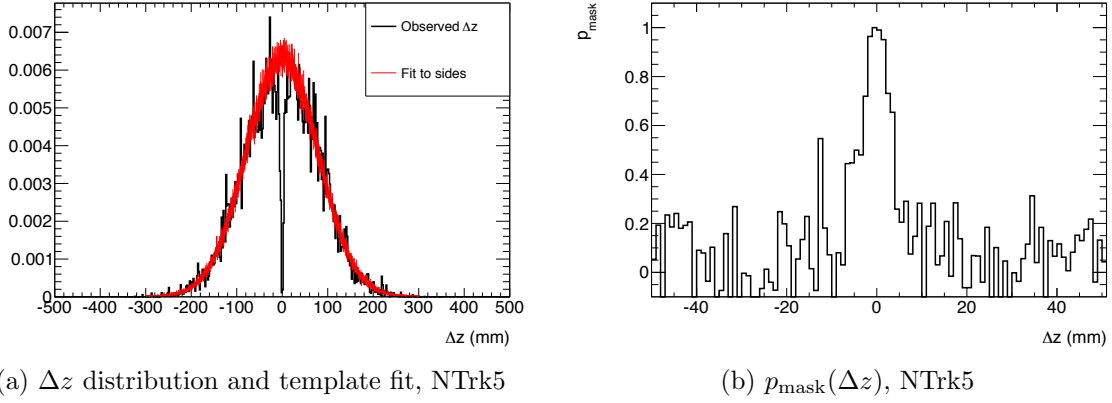


Figure 4.9: Calibration of the masking correction method on simulation, using 8 TeV minimum bias Monte Carlo (pythia 8, tune A2M). Left:  $\Delta z$  distributions and template fits using expected  $\Delta z$  distributions in the range  $30 \text{ mm} \leq \Delta z \leq 300 \text{ mm}$ . Right: pairwise vertex masking probability as a function of the longitudinal distance  $\Delta z$  between the vertices.

$$p_1 = 1 \quad (4.16)$$

$$p_2 = p_1 \times (1 - p_{\text{mask}}) \quad (4.17)$$

$$\dots \quad (4.18)$$

$$p_k = \prod_{i=1}^{k-1} (p_i \times (1 - p_{\text{mask}}) + (1 - p_i) \times 1) \quad (4.19)$$

$$= \prod_{i=1}^{k-1} (1 - p_i p_{\text{mask}}) \quad (4.20)$$

$$= p_{n-1} \times (1 - p_{n-1} p_{\text{mask}}) \quad (4.21)$$

The average number of reconstructed vertices is then:

$$\langle N_{\text{rec}} \rangle = \sum_{i=1}^{N_{\text{vis}}} p_i. \quad (4.22)$$

4. Finally, a map is computed between the average number of reconstructible vertices,  $\mu_{\text{vis}}$ , and the average number of reconstructed vertices,  $\mu_{\text{rec}}(\mu_{\text{vis}})$ , by convoluting  $\mu_{\text{rec}}(N_{\text{vis}})$  with a Poisson distribution:

$$\langle \mu_{\text{rec}} \rangle(\mu_{\text{vis}}) = \sum_{N_{\text{vis}}=0}^{\infty} P(N_{\text{vis}}; \mu_{\text{vis}}) \mu_{\text{rec}}(N_{\text{vis}}). \quad (4.23)$$

## Vertex-Based Luminosity Measurements in 2011

Due to the low event rate available during physics runs, vertex counting was used to measure luminosity only in three special runs during 2011, where inner detector data were recorded by a special high-rate data stream. The data stream reads out events at  $\mathcal{O}(10\text{ kHz})$ , recording only the inner detector from a small number of bunch crossings, typically less than four. The three runs are the vdM calibration run in May 2011, the pileup scan in September 2011 shown in figure 4.4b, and a high- $\beta^*$  run with a single bunch used to measure the total  $pp$  cross section using the ALFA detector.

### Van der Meer Scan

An example scan curve from the May 2011 vdM scan is shown in figure 4.10. The trigger used to collect the data required two hits in the MBTS, and selected 3 of the 14 colliding bunch pairs. The peak interaction rate during the fill was  $\mu \sim 2.3$ . The data are corrected for vertex masking and fakes, with the correction factor reaching up to 3% at the peak of the scan curves. Following the protocol described in section 4.4, the visible cross section is determined to be  $(38.50 \pm 0.12)$  mb, where the uncertainty reflects the RMS spread between the three bunch crossings and the two scans.

### Pileup Scan

The September 2011 pileup scan is used to derive systematic uncertainties due to the non-linear response of algorithms with respect to the number of interactions per bunch crossing. The scan was performed at the end of a physics run, displacing the beams in the transverse direction to obtain a sample of data at over a pileup range of  $0.02 \lesssim \mu \lesssim 10$  with otherwise identical conditions. The data was triggered by a random trigger selecting events from two BCIDs, 200 and 999. The data are corrected for vertex masking and fakes, with the correction reaching up to 10% as shown in figure 4.11 with respect to BCM\_VOR. A comparison of the luminosity measurements between vertex counting and BCM\_VOR, shown in figure 4.12, exhibits a slope of about 0.1% per unit of  $\mu$ .

### ALFA Run

Finally, vertex counting provides a reliable luminosity measurement for the 2011 ALFA run, a special run used for a measurement of the total  $pp$  cross section [13]. The beams contained a single colliding bunch pair with  $\beta^* = 90\text{ m}$  and  $\mu \sim 0.03$ , in order to measure the scattering angle of elastic  $pp$  collisions. A special luminosity analysis is required to address the very low instantaneous luminosity of  $\mathcal{L} \sim 5 \times 10^{27} \text{ cm}^{-2} \text{ s}^{-1}$ , about six orders of magnitude lower than a typical physics fill. The calorimeter methods are unusable due to a



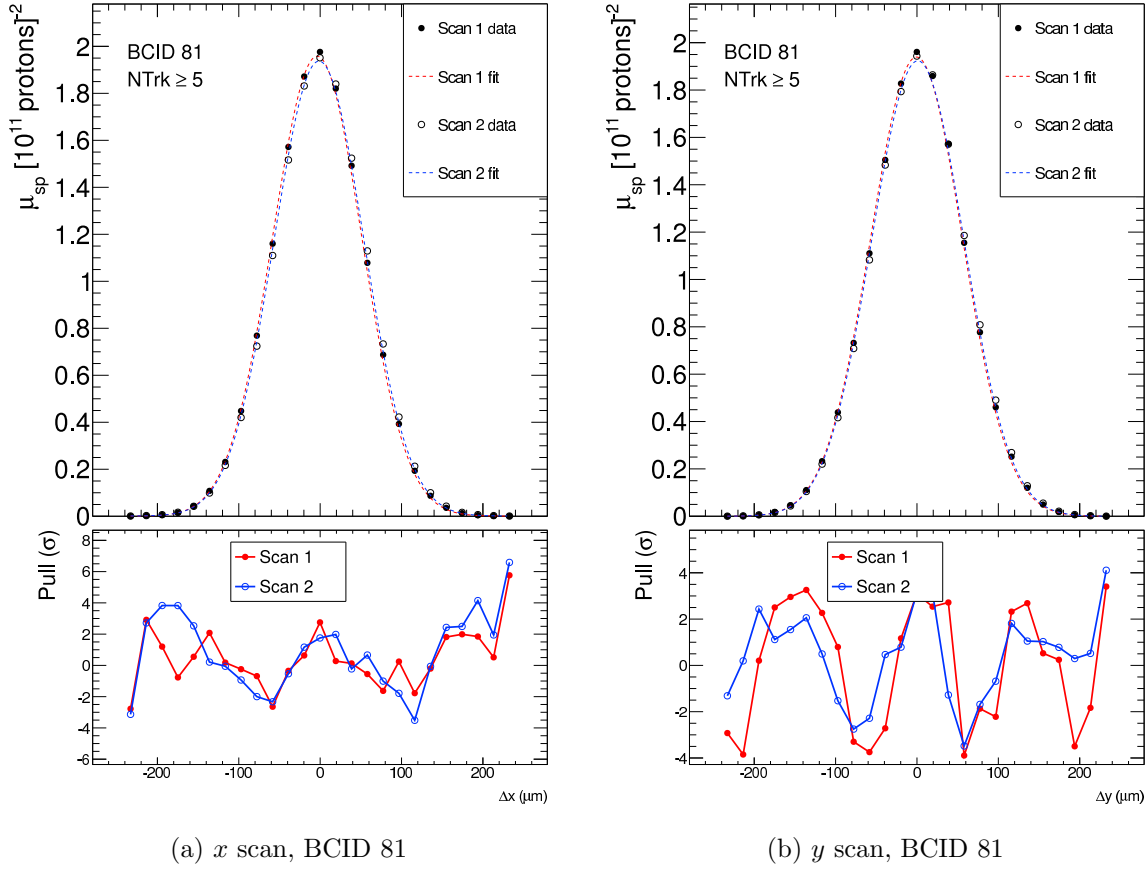
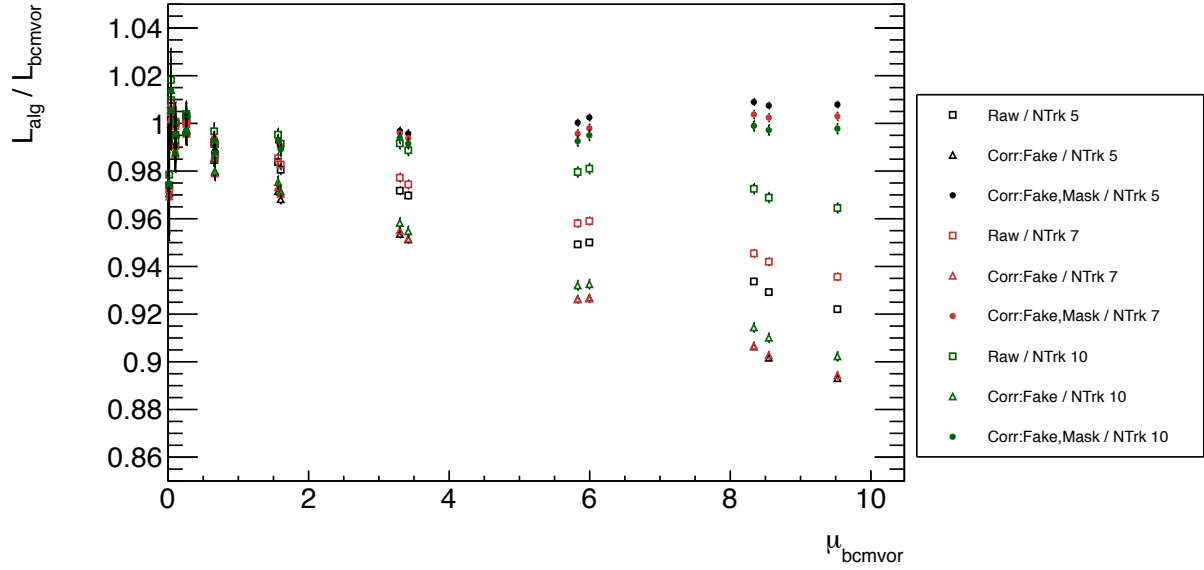


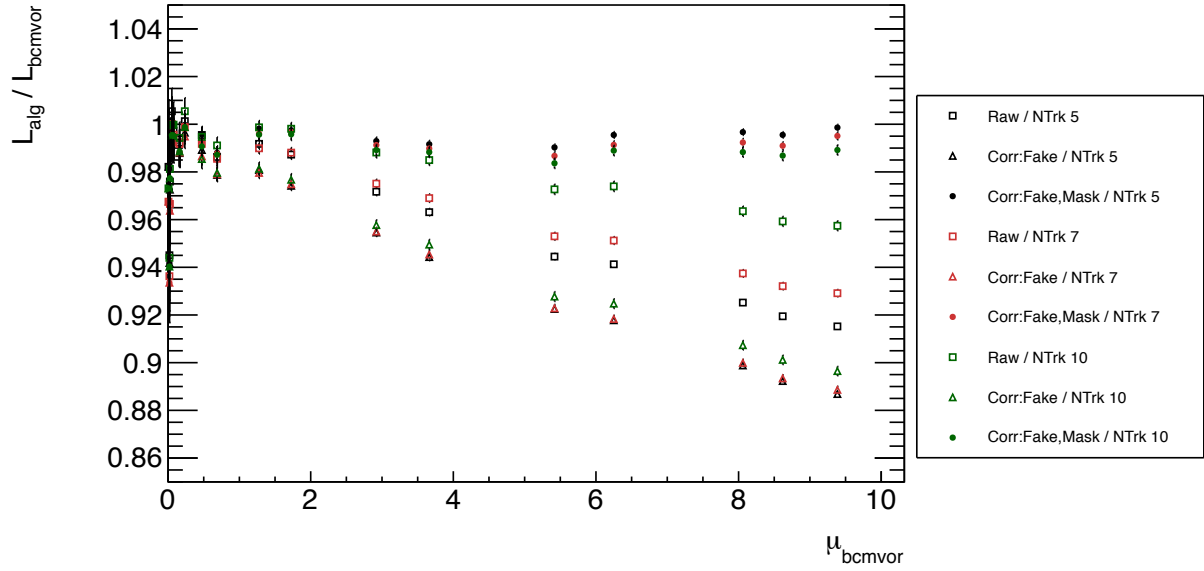
Figure 4.10:  $\mu_{\text{vis}}^{(sp)}$  vs. beam separation, with single gaussian plus constant fits, and pulls.

lack of sensitivity. For BCM and LUCID, the backgrounds at low instantaneous luminosity have a different composition: afterglow is negligible with a single colliding bunch, but beam-gas interactions can be significant, resulting in an extra 0.2% systematic uncertainty. The low-pileup conditions are ideal for vertex counting, eliminating the need to perform pileup corrections. The requirement of at least five tracks with  $p_T > 400$  MeV per vertex suppresses the beam-gas backgrounds. The data were recorded by a random trigger at approximately 1 kHz.

A comparison of luminosity measurements from BCM, LUCID, and vertex counting is shown in figure 4.13. To be consistent with the primary  $pp$  luminosity measurement, the central value is taken from BCM\_VOR; vertex counting shows agreement with this value to within 0.5%.



(a) BCID 200



(b) BCID 999

Figure 4.11: Ratio of luminosity values from vertexing to the reference value from BCM\_VOR during the pileup scan in September 2011. The black points show the vertex-based luminosity with  $\geq 5$  tracks, the red with  $\geq 7$  tracks, and the green with  $\geq 10$  tracks. The different shapes show the application of each successive pileup correction: the hollow squares show the vertex-based luminosity with no pileup corrections applied, the hollow triangles are corrected for fake vertices, and the solid circles are corrected for both fake and masked vertices.

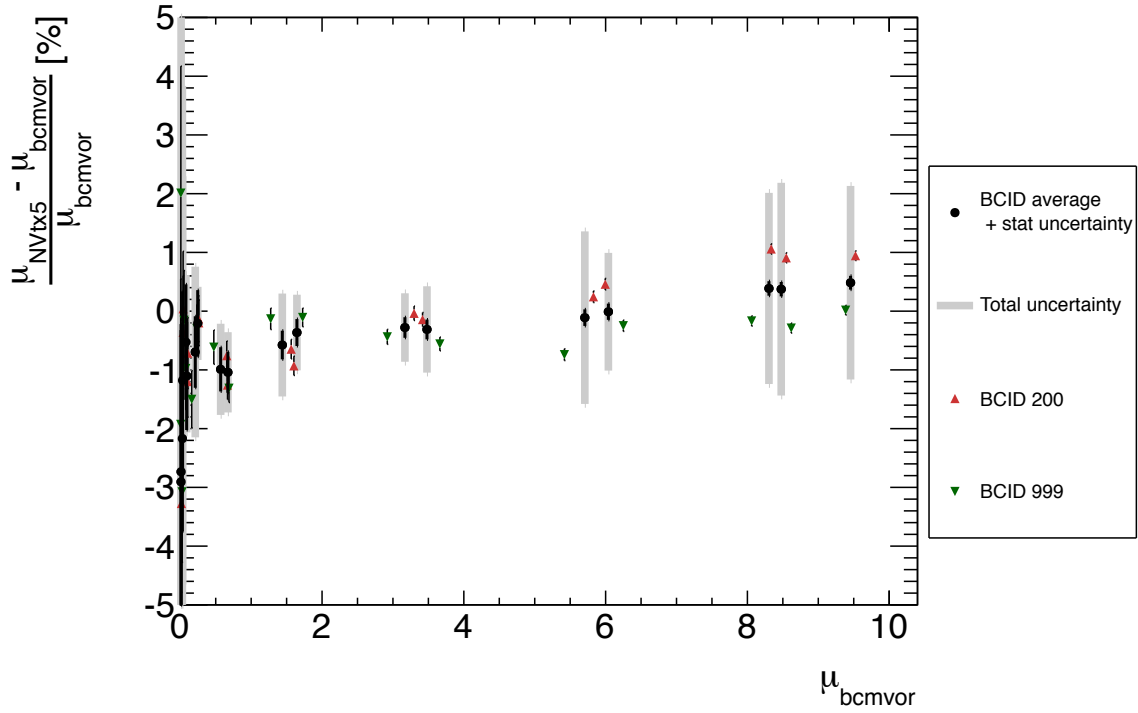


Figure 4.12: Percent difference between luminosities measured by vertex counting and BCM\_VOR during the pileup scan in September 2011. Vertices are required to have at least five tracks. The black points show the central values, taken to be the average between the two colliding BCIDs. The grey bars show the spread between BCIDs and between different track cuts ( $\geq 5$ ,  $\geq 7$ , and  $\geq 10$ ), summed in quadrature.

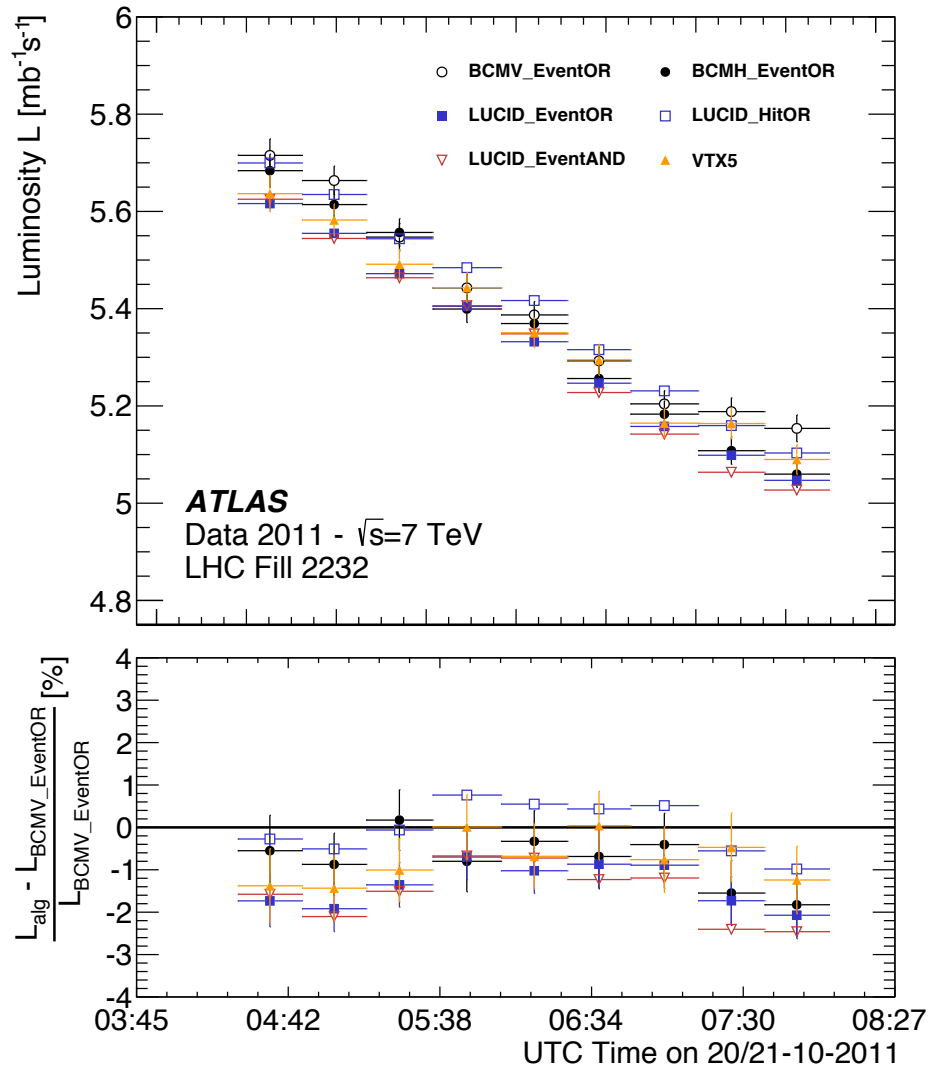


Figure 4.13: Luminosities measured by BCM, LUCID, and vertex counting during the  $\beta^* = 90$  m ALFA run in October 2011.

# Bibliography

- [1] P. Grafström and W. Kozanecki, *Luminosity determination at proton colliders*, Progress in Particle and Nuclear Physics (Jan. 2015) pp. 1–52.
- [2] The ATLAS Collaboration et al., *Improved luminosity determination in pp collisions at  $\sqrt{s} = 7$  TeV using the ATLAS detector at the LHC*, arXiv **C73.8** (2013) p. 2518, URL: <http://arxiv.org/abs/1302.4393>.
- [3] H. Fraiss-Kolbl, H. Fraiss-Koelbl, et al., *The ATLAS Beam Conditions Monitor*, English, JINST **3.02** (2008) P02004–P02004, URL: <http://stacks.iop.org/1748-0221/3/i=02/a=P02004?key=crossref.925163f83f527ab642c655fa05d88708>.
- [4] T. A. Collaboration, *The ATLAS Experiment at the CERN Large Hadron Collider*, Journal of Instrumentation **3.08** (Aug. 2008) S08003–438.
- [5] S. van der Meer, *Calibration of the Effective Beam Height in the ISR* (June 1968) pp. 1–4.
- [6] C. Barschel et al., *Results of the LHC DCCT Calibration Studies* (Feb. 2012), URL: <http://cds.cern.ch/record/1425904>.
- [7] G. Anders et al., *Study of the Relative LHC Bunch Populations for Luminosity Calibration* (Feb. 2012), URL: <http://cds.cern.ch/record/1427726>.
- [8] A. Alici et al., *Study of the LHC ghost charge and satellite bunches for luminosity calibration*. (Feb. 2012), URL: <http://cds.cern.ch/record/1427728>.
- [9] T. A. Collaboration, *Measurement of the total cross section from elastic scattering in pp collisions at  $\sqrt{s} = 7$  TeV with the ATLAS detector*, Nuclear Physics B **889.C** (Dec. 2014) pp. 486–548.
- [10] S. Pagan Griso, D. Yu, and B. Heinemann, *Luminosity Measurement in pp Collisions at  $\sqrt{s} = 7$  TeV using Vertex Counting with the ATLAS Detector in 2011* (July 2013) pp. 1–59.
- [11] T. Sjöstrand, S. Mrenna, and P. Z. Skands, *A Brief Introduction to PYTHIA 8.1*, Comput. Phys. Commun. **178** (2008) pp. 852–867, arXiv: 0710.3820 [hep-ph].

- [12] ATLAS Collaboration, *Summary of ATLAS Pythia 8 tunes* (2012).
- [13] The ATLAS Collaboration, *Measurement of the total cross section from elastic scattering in  $pp$  collisions at  $\sqrt{s} = 7$  TeV with the ATLAS detector*, Nuclear Physics B **889**.C (Dec. 2014) pp. 486–548,  
URL: <http://dx.doi.org/10.1016/j.nuclphysb.2014.10.019>.